Journal of the Brazilian Society of Mechanical Sciences and Engineering (2023) 45:80
https://doi.org/10.1007/s40430-022-04006-8

TECHNICAL PAPER

Experimental observation of ethanol–air premixed flames propagating inside a closed tube with high aspect ratio

Aguinaldo M. Serra Jr[1] · José C. Andrade[1] · Lucas M. Silva[2] · José C. Santos[1] · Julia C. Silveira[3] · João A. de Carvalho Jr[2,4] · Andrés Z. Mendiburu[3,4]

Received: 17 April 2022 / Accepted: 27 December 2022

Abstract

The present article aims to experimentally observe the flame propagation of ethanol–air mixtures in a tube closed at both ends with an aspect ratio of 27.68. The mixtures were prepared with equivalence ratios ranging from 0.8 to 1.1. The tests were performed for initial pressures of 20, 40, and 60 kPa. The phenomenon of flame front inversion was observed in all experiments. This phenomenon is also known as tulip flame. It was also observed that the flame front inverted several times at the equivalence ratios of 1.0 and 1.1. After the initial deceleration, the velocity oscillated with a high amplitude at these equivalence ratios. An analysis of the available experimental data was performed to better understand the conditions that allow the flame velocity oscillations to occur. It was found that these oscillations manifest when the following conditions are met: (a) closed channels, (b) sufficiently high laminar flame velocity and (c) sufficiently high aspect ratio. Moreover, this phenomenon is coupled with pressure waves that develop inside the duct. The relationship between the distance for the formation of the flattened flame front and the laminar flame velocity was used to define a characteristic time that correlates with the available experimental data.

Keywords Flame front inversion · Deflagrations · Closed tubes · Ethanol

List of symbols

AR	Aspect ratio
c_p	Heat capacity at constant pressure (J/kg K)
d	Tube diameter (m)
d_f	Distance of flattened flame formation (m)
E_a	Activation energy (J/mol)
t_{flat}	Characteristic time (s)
L	Tube or duct length (m)
p	Pressure (kPa)
Δp	Pressure increase (kPa)
p_v	Pressure after vacuum (kPa)
$p_{F,i}$	Apparent fuel pressure (kPa)
p_F	Real fuel pressure (kPa)
p_{air}	Real air pressure (kPa)
R	Universal gas constant (J/mol K)
s_L	Laminar burning velocity (m/s)
Δs_L	Relative increase of laminar flame velocity (%)
t_{flat}	Characteristic time for flattened flame formation (s)
T_b	Adiabatic flame temperature
V	Axial velocity of the flame tip (m/s)
x	Axial coordinate position (m)

Greek letters

ϕ	Equivalence ratio
ω	Uncertainty of a physical quantity
λ	Thermal conductivity (W/m)

Subscripts

b	Conditions in the burned gases
h	Hydraulic diameter

Technical Editor: Mario Eduardo Santos Martins.

✉ Andrés Z. Mendiburu
andresmendiburu@ufrgs.br

[1] Combustion and Propulsion Laboratory, National Space Research Institute (INPE), Rod. Pres. Dutra, km 39, Cachoeira Paulista, SP CEP 12630-000, Brazil

[2] Department of Chemistry and Energy, School of Engineering, São Paulo University (UNESP), Guaratinguetá, Av. Ariberto P. da Cunha, 333, Guaratinguetá, SP CEP 12510410, Brazil

[3] Department of Mechanical Engineering, Federal University of Rio Grande do Sul (UFRGS), R. Sarmento Leite 425, Porto Alegre, RS CEP 90050-170, Brazil

[4] International Research Group for Energy Sustainability (IRGES), R. Sarmento Leite 425, Porto Alegre, RS CEP 90050-170, Brazil

Published online: 11 January 2023

1 Introduction

Research on ethanol combustion is important because it is a fuel that can be derived from biomass such as corn in the USA and sugarcane in Brazil. Taking gasoline as the base fuel, life cycle assessment has shown that ethanol from sugarcane has the potential to reduce CO_2 equivalent emissions by 67% to 80% [1–3]. Life cycle assessment has also shown that ethanol from sugarcane produces 17.3 g-CO2eq/MJ-ethanol, compared to 56.6 g-CO2eq/MJ-ethanol when produced from corn [4]. Therefore, ethanol produced from sugarcane is a particularly important biofuel for reducing greenhouse gas emissions.

Observing the propagation of premixed flames in ducts and tubes is important to the process industry because the flames are greatly accelerated in the early stages of propagation and undergo further acceleration in the presence of obstacles. Also, the phenomenon of flame front inversion and the high amplitude velocity fluctuations observed after the initial front inversion are relevant to the industry due to coupling with pressure waves within the tubes.

In previous work, the authors have studied various combustion properties of ethanol, for example, flammability limits [5, 6] and detonation limits [7]. The flame propagation of ethanol in a closed tube is also an important phenomenon, since under such conditions the flame exhibits acceleration in the early stages of the process, as described by Valiev et al. [8]. Flameless combustions [9] and the instability of the premixed flame front of ethanol [10] have been investigated by other authors.

In general, the propagation of a premixed flame in a closed tube (or duct) can be divided into four main processes: (a) spherical flame propagation, (b) flame acceleration in the axial direction, (c) flame front inversion, (d) cellular flame propagation. The phenomenon of flame front inversion is also called tulip flame [11]. The aspect ratio of the tube (AR) plays an important role in the formation of the tulip flame. It is defined as the ratio of the tube length (L) to the tube diameter (d). It is an empirical rule that the aspect ratio must be greater than two to observe a tulip flame [11, 12].

The tulip flame phenomenon occurs when a premixed flame spreads in a tube (or duct) that is closed at both ends or only at the ignition end. Therefore, this phenomenon can also occur in half-open tubes. There are three instabilities associated with premixed flame propagation, namely, buoyancy-driven instability (Rayleigh–Taylor), diffusive-thermal instability, and hydrodynamic (Darrieus–Landau) instability [13, 14]. According to Ponizy et al. [15], the tulip flame is formed because a backward flow of burned gasses is formed and there is competition between the forward flow of unburned gasses and the backward flow of burned gasses.

The theoretical explanation for the acceleration of the early stages of flame propagation in a closed tube was developed by Valiev et al. [8]. Although the theory approximates the time at which the flame contacts the side walls of the tube with good accuracy, it is not quantitatively accurate in determining the flame speed. Other theoretical works that also focus on the early acceleration stage are those of Akkerman et al. [16] and by Bychkov et al. [17, 18]. To the authors' knowledge, there is no analytical theoretical development that considers the deceleration stage.

The phenomenon of tulip flame has been studied experimentally for various fuels. For example, Xiao et al. [19–24] and Shen et al. [25] studied hydrogen–air mixtures. Zheng et al. [26] and Yu et al. [27, 28] studied hydrogen–methane–air mixtures. Yu et al. [29, 30] studied carbon monoxide–hydrogen–air mixtures. Hariharan and Wichman [31, 32] investigated methane–air mixtures. Jin et al. [33] studied natural gas–air, methane–air, and acetylene–air mixtures. Dunn-Rankin and Sawyer [34] studied methane–air and ethylene–air mixtures. Ponizy et al. [15] also investigated propane–air mixtures.

Although the phenomenon of flame front inversion has been observed in ducts closed at both ends and in ducts closed only at the ignition end, there is a marked difference in the behavior of the flame speed in these configurations. This difference is that the flame velocity oscillates at high amplitudes for channels closed at both ends compared to channels closed only at the ignition end. As far as the authors are aware, the variables associated with the occurrence of these velocity oscillations have not been clearly addressed in the literature on tulip flames. A comparison of the studies performed by Yu et al. [29, 30] and by Yang et al. [35, 36] with the results obtained in the present work will provide the necessary evidence to identify the variables causing the strong oscillations in flame velocity.

Various tube configurations have been studied experimentally and numerically. For example, there is evidence that bent tubes can produce higher flame acceleration [37]; however, the bent could be considered as an obstacle that promotes flame acceleration. Therefore, a bent tube would not be suitable to study the flame inversion phenomenon. Numerical simulations have shown that a flame propagating in a tube with different contraction angles has six stages. Among these stages, the spherical flame, the finger flame, the flame touching the side walls, and the tulip flame are observed [38]. Therefore, the phenomenon of flame front inversion is also relevant to tubes that transition into different cross sections.

In the present work, the propagation of ethanol–air flames in a closed tube with high aspect ratio (27.68) is studied. In a previous study [39], the authors observed flame front inversion of ethanol–air mixtures in a tube with an aspect ratio of 15.46. As far as the authors are aware, there are no

published articles dealing with the formation of tulip flames from ethanol in a closed tube with a high aspect ratio. Also, most of the experimental data available for other fuel–air mixtures have been obtained in tubes with moderate aspect ratios (less than 15). Experiments considered initial pressures of 20, 40, and 60 kPa and equivalence ratios of 0.8 to 1.1. When this work refers to a half-open tube (or duct), it means that the tube is closed at the ignition end and open at the opposite end.

2 General behavior and theoretical analysis

It is interesting to describe first the general behavior of a deflagration propagating in a tube closed at both ends or only at the ignition end (half-open). After ignition, a first stage of spherical flame propagation takes place. The second stage, referred to in the literature as finger flame propagation [15], is the stage in which higher acceleration occurs due to the increasing flame surface area. At a certain point, the flame touches the side walls of the tube and the third stage begins. In the third stage, the flame has consumed all the mixture in the radial direction up to the axial distance traveled, so the flame surface begins to decrease, and the flame slows down. In this phase, the backward movement of the combustion products starts, but far from the flame front, as described by Ponizy et al. [15]. At a certain point in the slowing down process, the flame front becomes almost flat.

At the fourth stage, the flame front begins to reverse, and the tulip flame is formed. The central part of the flame front moves slower or even backwards compared to the lateral parts of the flame front. The tulip flame propagates until the instant when the central part collapses and the front is no longer inverted. Finally, cellular flame propagation occurs until the flame has traveled the available distance inside the tube. The phenomenon described up to this point is also observed in tubes or ducts with lower aspect ratio.

The flame acceleration stage can be studied using the theoretical approaches developed by several authors [11, 16–18]. The theoretical developments of Valiev et al. [8] take into account the first two stages of flame propagation mentioned above and can determine the time at which the third phase starts. This theory is considered for the calculations in this paper. The solution presented here is for an axisymmetric geometry. In their work, Valiev et al. obtained the solution also for a planar geometry. The dimensionless parameters are the dimensionless time ($\tau = s_L t/R$), the dimensionless axial coordinate ($\xi = x/R$), the expansion ratio of the gas ($\Theta = \rho_u/\rho_b$), the initial Mach number ($Ma = s_L/C_{s,0}$) and the ratio of heat capacities ($\gamma = c_p/c_v$). Combinations of these variables define some auxiliary parameters required to perform the calculations. These are given in Eqs. (1) to (5).

$$\alpha = \sqrt{\Theta(\Theta-1)};\ \ \alpha_1 = \sqrt{\Theta_1\left(\Theta_1-1\right)} \tag{1}$$

$$\Theta_1 = \Theta - \mathrm{Ma}(\gamma-1)(\Theta-1)^2;\ \ B = (\gamma-1)(\Theta-1)(2\Theta-1) \tag{2}$$

$$\sigma_1 = (\Theta-1)\{1-\mathrm{Ma}[\Theta+2(\gamma-1)(\Theta-1)]\} \tag{3}$$

$$\sigma_{1,\mathrm{axi}} = 2\alpha\left\{1-\mathrm{Ma}\left[\Theta+\left(2-\frac{1}{2\Theta}\right)(\gamma-1)(\Theta-1)\right]\right\} \tag{4}$$

$$\sigma_2 = \sqrt{\sigma_{1,\mathrm{axi}}^2 + 4\Theta_1 \mathrm{Ma}\psi},\ \ \psi = 2(\Theta-1)(2\Theta\gamma-\gamma+1) \tag{5}$$

The time at which the flame skirt reaches the side walls of the tube in an axisymmetric geometry is determined by Eq. (6) according to [8, 17]. The velocity of the flame tip is determined by Eq. (7). However, the position of the flame tip is required to use this expression.

$$\tau_{\mathrm{wall}} = \frac{1}{2\alpha}\ln\left(\frac{\Theta+\alpha}{\Theta-\alpha}\right) \tag{6}$$

$$\begin{aligned}\frac{\mathrm{d}\xi_{\mathrm{tip}}}{\mathrm{d}\tau} &= \left\{2\alpha_1\tanh\left(\alpha_1\tau\right) - 2\mathrm{Ma}\times\alpha[1+\gamma(\Theta-1)]\right\}\xi_{\mathrm{tip}} \\ &+ \Theta_1 - 2\mathrm{Ma}\left\{\frac{\alpha\tau B}{\cosh^2(\alpha\tau)} + \left(2\alpha^2-B\right)\tanh\alpha\tau\right\}\xi_{\mathrm{tip}}^2\end{aligned} \tag{7}$$

Therefore, Eq. (7) must be solved to obtain the position of the flame tip as a function of time. The analytical solution of Valiev et al. considers two limiting cases, the first limiting case being for an incompressible flow. The determined position of the flame tip is given by Eq. (8). The second limiting case concerns a late stage of flame acceleration, and the position of the flame tip is determined by Eq. (9).

$$\begin{aligned}\xi_{\mathrm{tip},1} = \frac{\Theta_1}{2\alpha_1}\sinh\left(2\alpha_1\tau\right) - 2\mathrm{Ma}\frac{\Theta}{\alpha}[1+\gamma(\Theta-1)] \\ \cosh^2(\alpha\tau)\ln[\cosh(\alpha\tau)]\end{aligned} \tag{8}$$

$$\xi_{\mathrm{tip},2} = \frac{2\Theta_1\left[\exp\left(\sigma_2\tau\right)-1\right]}{\left(\sigma_2-\sigma_{1,\mathrm{axi}}\right)\exp\left(\sigma_2\tau\right)+\left(\sigma_2+\sigma_{1,\mathrm{axi}}\right)} \tag{9}$$

The maximum flame tip velocities corresponding to the above flame tip positions are given in Eqs. (10) and (11).

$$\begin{aligned}U_{\mathrm{max},1} = \frac{V_{\mathrm{tip},1}}{s_L} = \left\{2\alpha_1\tanh\left(\alpha_1\tau_{\mathrm{wall}}\right) - 2\mathrm{Ma}\right. \\ \left.\times\alpha[1+\gamma(\Theta-1)]\right\}\xi_{\mathrm{wall},1} + \Theta_1\end{aligned} \tag{10}$$

$$U_{\max,2} = \frac{V_{\text{tip},2}}{s_{\text{L}}} = -2\text{Ma}(\Theta - 1)(2\Theta\gamma - \gamma + 1)\xi^2_{\text{wall},2} + \sigma_{1,\text{axi}}\xi_{\text{wall},2} + \Theta_1 \quad (11)$$

The equations in this section allow to determine the maximum velocity of the flame tip inside the tube, the time at which the flame skirt touches the side walls of the tube, and the position of the flame tip at that time.

3 Experimental setup

3.1 Experimental procedure

The experimental setup mainly consisted of a mixing chamber, a flame propagation tube, a high-speed camera, an ignition system, a vacuum pump, and a data acquisition system. The experimental setup is schematically shown in Fig. 1. The mixing chamber consists of a spherical borosilicate vessel contained in a stainless-steel box. The vessel has a volume of 20 L and is equipped with a 2 bar pressure sensor and a type K thermocouple. The stainless-steel box is equipped with a window to check the evaporation of the ethanol, electrical resistors to heat the ethanol–air mixture to temperatures around 50 °C, a thermocouple to monitor the temperature, a temperature controller and a small fan to distribute the warm air in the box. A magnetic stirrer was used to improve the ethanol–air mixing process.

The propagation tube consists of two borosilicate tubes with a diameter of 97 mm. The length of these tubes is 150 cm and 105 cm, respectively. The tubes are connected by a joint designed and built for this purpose; the total length of the propagation tube is 268.5 cm. The borosilicate tubes provide a wide field of view for the experimental tests. The propagation tube is equipped with a thermocouple and two pressure transducers of 10 bar and 2 bar, respectively.

A FasTec TS3 video camera was used to record flame propagation inside the tube during the tests. The data were recorded by an acquisition system connected to a personal computer. The ignition system consisted of a transformer and electrodes. The transformer supplied a voltage of 15 kV and a current of 30 mA to the electrodes.

The ethanol–air mixture was prepared in the mixing chamber by the partial pressure method. For this purpose, the vacuum pump was used to evacuate the spherical vessel to a pressure not exceeding 0.5 kPa. Then, the steel bottle containing the ethanol was opened and the ethanol was added to the container by first passing it through a heater to ensure its evaporation. Just before the desired partial pressure was reached, the ethanol inlet was closed. Through the window, it was possible to visually check whether the ethanol had completely evaporated or not.

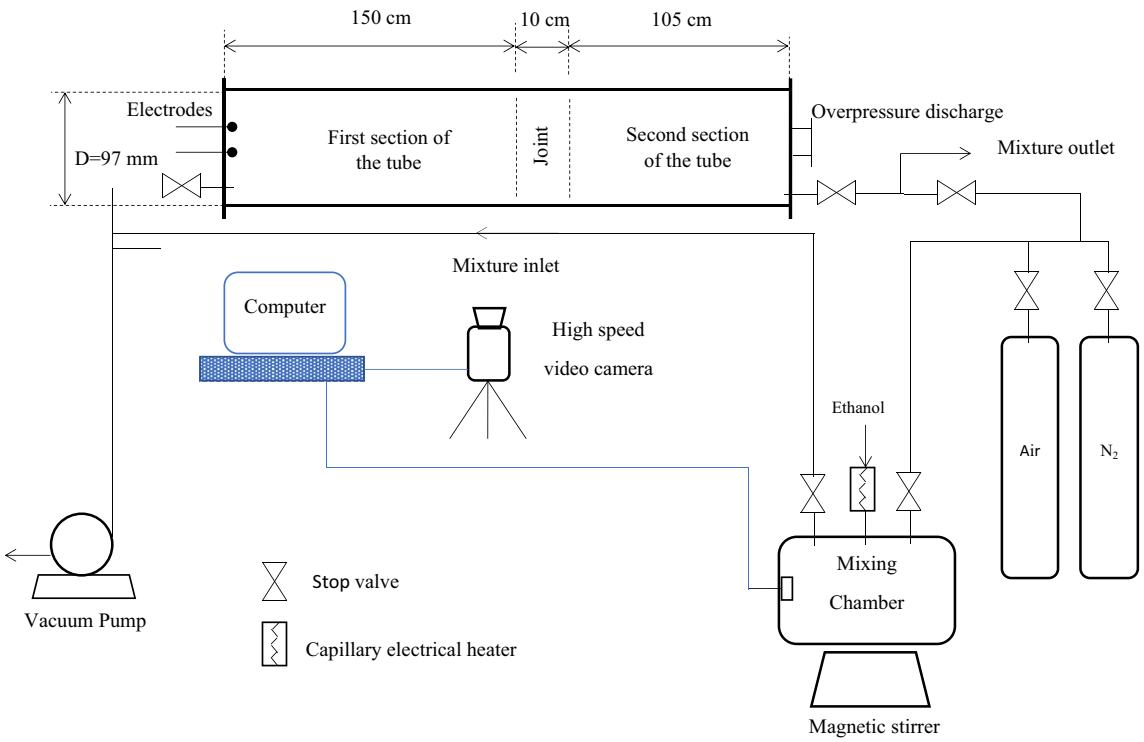

Fig. 1 Schematic diagram of the experimental apparatus

After the ethanol had completely evaporated, the air valve was opened and the spherical container was filled with air until the desired total pressure was reached. Generally, the total pressure in the mixing chamber was about 150 kPa. Once the mixture was prepared, the magnetic stirrer was operated for 25 min to ensure a homogeneous mixture. The mixture prepared in this way was sufficient for two consecutive flame propagation tests. The same mixing time was successfully used by the authors in a previous work [39]. In addition, it is important to note that experiments to determine the flammability limit according to the ASTM E681 standard [40] are performed with mixing times of less than 5 min after the gasses are admitted into the spherical vessel [6]. Therefore, the time of 25 min is considered sufficient to ensure a homogeneous mixture.

While the magnetic stirrer homogenized the ethanol–air mixture, the vacuum pump evacuated the propagation tube to a pressure not exceeding 0.5 kPa. Once the mixture was ready, it was allowed to enter the propagation tube to the desired initial pressure. Since the tube was not heated, the ethanol–air mixture was not allowed to rest for more than 30 s before ignition. Flame propagation was recorded by the high-speed video camera and pressure data was recorded by the data acquisition system.

After each propagation test, the burned gasses inside the tube were forced out through a release valve using nitrogen. Then the vacuum pump removed the remaining gasses inside the tube. This procedure was repeated at least twice before another test was performed. An analogous procedure was used in the mixing chamber once the ethanol–air mixture was insufficient to perform another test. The initial temperature inside the tube was 32 ± 5 °C.

The videos obtained from the experimental tests were processed using Tracker software [41] to obtain the axial velocity of the flame tip at different locations in the tube. The obtained flame velocities were divided by the laminar burning velocity (s_L) to obtain a dimensionless flame velocity. The laminar flame velocities were determined using Cantera software [42]. The kinetic mechanism for ethanol combustion developed by Marinov [43] was used in the simulations. The experimental determination of s_L was beyond the scope of the present work. Nevertheless, the mechanism developed by Marinov is accurate to determine the s_L and ignition delay time, as evaluated by Mendiburu et al. [44].

3.2 Uncertainty analysis for mixture preparation

Mixture preparation by the partial pressure method is a well-established procedure in experimental work on the propagation of premixed flames in tubes [7, 45] and on the determination of flammability limits in spherical vessels [46, 47]. Note that the real fuel pressure (p_F) after the addition of fuel is $p_F = p_{F,i} - p_v$, where $p_{F,i}$ is the apparent fuel pressure and p_v is the pressure after vacuum. On the other hand, the actual air pressure (p_{air}) is $p_{air} = p_T - p_{F,i} - p_v$. Where p_T is the total pressure of the mixture in the mixing chamber. The number of moles of fuel (n_F) and oxygen (n_{O2}) in the mixture is determined by Eqs. (12) and (13), respectively.

$$n_F = \frac{(p_{F,i} - p_v)V}{RT} \tag{12}$$

$$n_{O_2} = \frac{0.21(p_T - p_{F,i} - p_v)V}{RT} \tag{13}$$

The number of moles of oxygen at the stoichiometric composition per mole of fuel can be determined as given in Eq. (14) [48]. Therefore, the equivalence ratio is as shown in Eq. (15).

$$\frac{n_{O_2,stq}}{n_F} = x_C + 0.25x_H - 0.5x_O \tag{14}$$

$$\phi = \frac{n_{O_2,stq}}{n_{O_2}} = \left(\frac{x_C + 0.25x_H - 0.5x_O}{0.21}\right)\frac{p_{F,i} - p_v}{p_T - p_{F,i} - p_v} \tag{15}$$

Following Hollman [49], the uncertainty of the equivalence ratio of the mixture is determined by applying the partial derivatives of ϕ with respect to p_T, $p_{F,i}$ and p_v. The uncertainty is then calculated by Eq. (16).

$$\omega_\phi = \left[\left(\frac{\partial\phi}{\partial p_T}\omega_T\right)^2 + \left(\frac{\partial\phi}{\partial p_F}\omega_{F,i}\right)^2 + \left(\frac{\partial\phi}{\partial p_v}\omega_v\right)^2\right]^{1/2} \tag{16}$$

where,

$$\frac{\partial\phi}{\partial p_T} = -K\frac{p_{F,i} - p_v}{(p_T - p_{F,i} - p_v)^2} \tag{17}$$

$$\frac{\partial\phi}{\partial p_{F,i}} = K\frac{p_T - 2p_v}{(p_T - p_{F,i} - p_v)^2} \tag{18}$$

$$\frac{\partial\phi}{\partial p_T} = -K\frac{p_T - 2p_{F,i}}{(p_T - p_{F,i} - p_v)^2} \tag{19}$$

$$K = \frac{x_C + 0.25x_H - 0.5x_O}{0.21} \tag{20}$$

The uncertainties of the piezoelectric pressure sensors were 0.05% of full scale. Thus, for the 2 bar (200 kPa) pressure sensor used to prepare the mixture,

the uncertainty was 0.06 kPa. For ethanol, the constant value is $K = 14.286$. Let us assume the case when the desired equivalence ratio is $\phi = 0.80$, the $p_v = 0.5$ kPa, the $p_{F,i} = 94$ kPa and $p_T = 1501$ kPa. Then the value of experimental uncertainty is $\omega_\phi = 0.014$, which means that $\phi = 0.80 \pm 0.014$ in this case. For all considered equivalence ratios, the uncertainty with respect to the equivalence ratio was about 0.014.

4 Results and discussions

Flame propagation of ethanol–air mixtures in a closed tube was observed for equivalence ratios of 0.8 to 1.1 and initial pressures of 20 to 60 kPa. The results presented in this section correspond to representative experiments. However, the experiments were performed at least three times for each initial condition. It is important to note that experiments were also performed for an equivalence ratio of 0.7, but the flame is barely observable under this condition, so these results are not presented.

Figure 2 shows the propagation of a premixed ethanol–air flame with an equivalence ratio of 1.0 and an initial pressure of 60 kPa. The behavior observed in Fig. 2 is similar to that described in Sect. 2. However, the high aspect ratio of the tube causes the formation of three tulip flames up to the first 150 cm of the tube length. A fourth acceleration and deceleration process is observed between the first and second tulip flames, which is why four "hills" are seen in Fig. 3. This acceleration and deceleration process occurred between Fig. 2f and g. However, it was not identified as a tulip flame because a new finger flame formed after deceleration instead of the flame front inversion. Therefore, the process can be divided as follows:

1. *Spherical flame propagation* it is related to the position of the ignition source. The spherical flame propagates radially until one side touches the closed end near to ignition source. The end of this stage is shown in Fig. 2a.
2. *Finger flame propagation* it is related to the significant flame acceleration in the axial direction. The flame acceleration is possible due to the increasing flame surface and continues until the flame skirt touches the side walls of the tube. The first, second, and third stages of finger flame propagation are shown in Fig. 2b, g, and j, respectively. There is a fourth stage of finger flame propagation between Fig. 2f and g that is not shown in Fig. 2.
3. *Flattened flame front formation* it is related to the significant flame deceleration on the axial direction. Once the mixture is completely burned in the radial direction near the ignition source, the flame surface area decreases as more mixture is burned in the radial direction. This phase also begins the backward movement of the com-

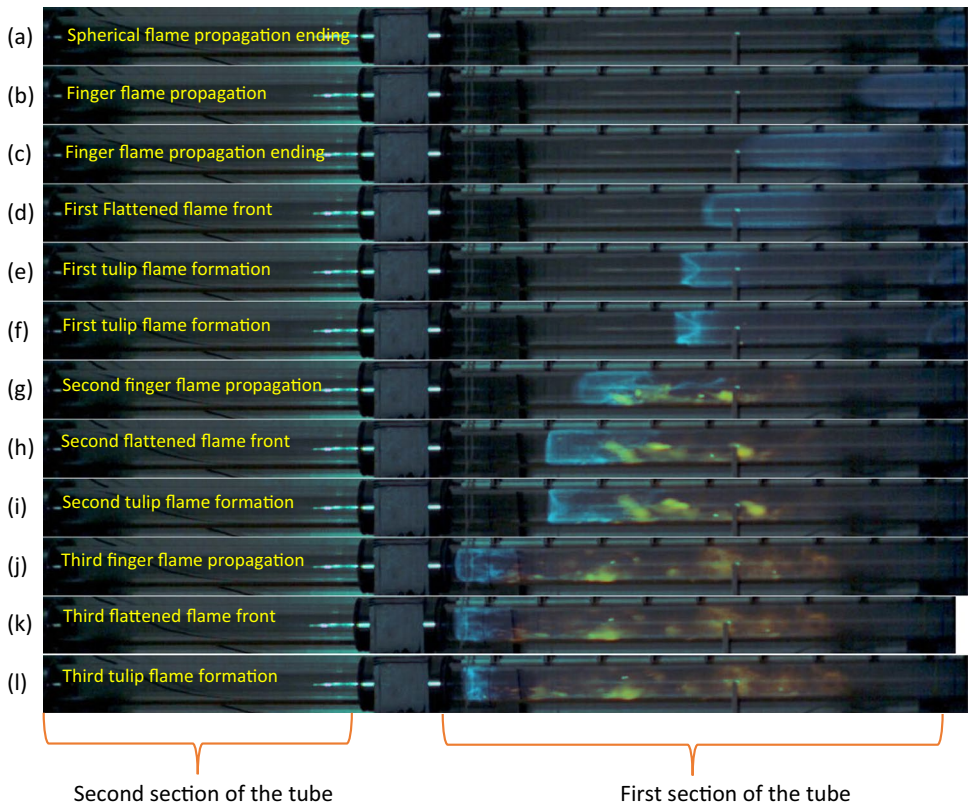

Fig. 2 Images extracted from video of tests #36 for ethanol–air mixture with $\phi = 1.0$ and $p_i = 60$ kpa

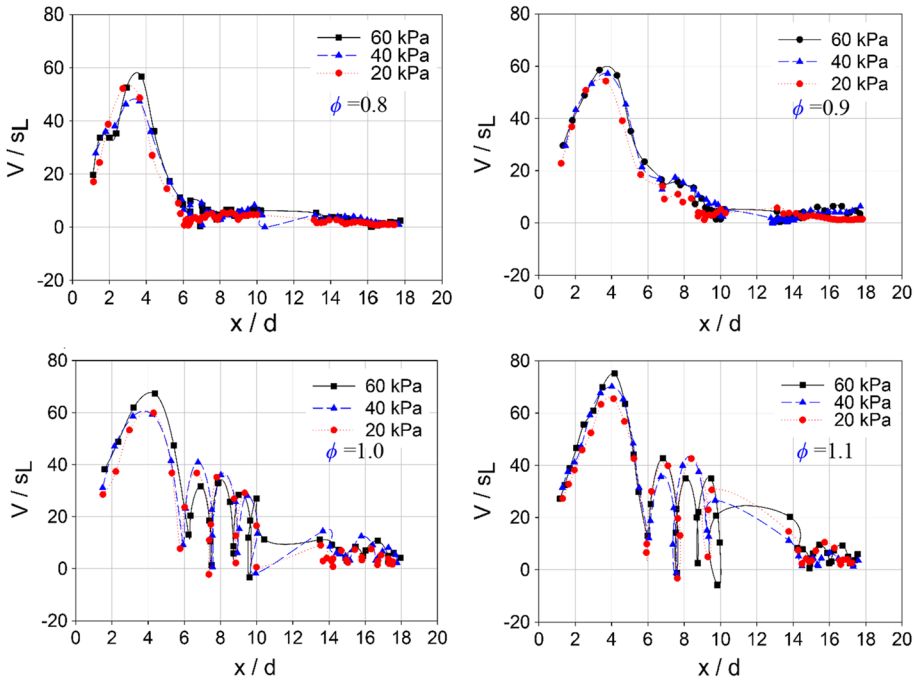

Fig. 3 Experimental results of the flame velocity along the tube axis for different equivalence ratios and initial pressures

bustion products due to the increasing pressure in front of the flame surface. The first, second and third onset of this phase can be seen in Fig. 2d, h and k, respectively.

4. *Tulip flame formation* it is related to the backward movement of the combustion products, especially near the central part of the flame front. The flame front inverts and assumes a tulip-like shape. The central part of the tulip flame will eventually collapse. The first, second, and third tulip flame shapes can be seen in Fig. 2e, i, and l, respectively.
5. *Cellular flame propagation* It is related to the interaction of the flame front with the acoustic waves generated inside the tube. This stage occurs after the last inversion of the flame front and continues until the flame reaches the end of the tube. This phase is not shown in Fig. 2.

Flame propagation in the second section of the tube, which is 105 cm long, was not shown in Fig. 2. In this section of the tube, the flame propagates at a much slower rate than in the finger flame propagation. The flame front has a cellular pattern, which is related to the interaction with the acoustic waves generated inside the tube [50].

The flame velocities along the tube axis were determined from the different videos of the experimental tests using the Tracker software [41]. Figure 3 shows the velocities obtained at different initial pressures and equivalence ratios. The axis of the plots shown in Fig. 3 corresponds to the dimensionless distance defined as the ratio between the distance traveled by the flame tip and the tube diameter (x/d), while the ordinate represents the dimensionless velocity defined as the ratio between the flame tip velocity and the calculated laminar flame velocity (V/s_L).

In the diagrams corresponding to the equivalence ratios of 0.8 and 0.9, it can be observed that the central part of the flame accelerates until it reaches a maximum velocity corresponding to about 50 to 60 times the laminar burning velocity. After that, the central part of the flame starts decelerating until it reaches a state where the velocity oscillates several times within a certain range. For example, for the experiment at 60 kPa and $\phi = 0.8$, the dimensionless velocity (V/s_L) oscillates between 0.33 and 9.86 for the dimensionless axial positions (x/d) between 5.99 and 10.20. In the later stages of the flame propagation process, the velocity of the flame tip is about two times the laminar burning velocity.

On the plots corresponding to the equivalence ratios of 1.0 and 1.1 for the different initial pressures, the behavior is qualitatively analogous, but with different values for the amplitude of the oscillations. Initially, the flame accelerates until it reaches velocities between 60 and 80 times the laminar flame velocity. Then the flame begins to decelerate and the velocity of the flame exhibits significant oscillations. For example, in the test with 60 kpa and $\phi = 1.1$, the dimensionless velocity oscillates in an interval from 2.59 to 42.72, while the flame propagates from 5.97 to 9.75 at the dimensionless axial positions. It can also be observed that the central part of the flame moves backward at certain times, generating negative velocities. In the final stages of flame propagation, the velocity of the central portion of the flame is approximately two to five times the laminar burning velocity.

Note that the point tracked to determine the propagation velocity is on the centerline of the flame front, and this point may move backward for a short time due to the inversion of the flame front, as is the case for $\phi = 1.1$ at 60 kPa near $x/d = 10$ (see Fig. 3). In most cases, however, this point continues to move in the direction of the flame propagation, albeit at a slower rate.

Thus, while at the equivalence ratios of 0.8 and 0.9 the velocity oscillations of the flame are small, it is observed that at the equivalence ratios of 1.0 and 1.1 the velocity oscillations have larger amplitudes. This phenomenon appears to be independent of the initial pressure, as it occurred for the three initial pressures considered in this work, as shown in Fig. 3. In the work of Shen et al. [51], this type of flame velocity oscillations also occurred for hydrogen–air mixtures in a closed channel with AR = 12 and for initial pressures of 0.6 and 1.4 atm. On the other hand, the amplitudes of the oscillations were moderate at a pressure of 0.3 atm. Thus, the initial pressure may or may not affect the occurrence of the high amplitude flame velocity oscillations depending on the fuel–air mixture.

A comparison between the flame velocities along the tube axis obtained in the present work with AR = 27.68 and those obtained in our previous work with AR = 15.46 [39], is shown in Fig. 4. It can be observed that for $\phi = 0.9$ the behavior is similar; however, for $\phi = 1.0$ the behavior is significantly different after the first deceleration. Although not shown in Fig. 4, the behavior for ER = 1.1 inside the tubes with AR = 27.68 and AR = 15.46 is also significantly different after the flame reaches its maximum velocity.

It is interesting to note which variables and conditions are relevant to the manifestation of the observed high amplitude flame velocity variations. The following variables are considered: (a) equivalence ratio, (b) boundary conditions (closed duct or half-open duct), (c) internal pressure, (d) aspect ratio, and (e) distance to flattened flame formation.

4.1 Equivalence ratio

Experimental observations show that the behavior of flame propagation in a closed tube with a high aspect ratio (AR = 27.68) depends strongly on the equivalence ratio of the mixture. The high amplitude flame velocity oscillations were observed for stoichiometric and slightly rich mixtures and not for lean mixtures. Therefore, the occurrence of these oscillations depends on the equivalence ratio. This conclusion is confirmed by the work of Shen et al. [52], who observed high amplitudes of flame velocity oscillations for hydrogen–air mixtures with $\phi = 1.17$ and moderate oscillations for mixtures with $\phi = 4.10$ and $\phi = 5.07$. Therefore, mixtures that are too lean or too rich do not show the high amplitude oscillations.

The observations regarding the equivalence ratio can be translated into a difference in laminar flame velocity (s_L) between the mixtures. The consideration is important when comparing different fuels or different fuel mixtures. In this

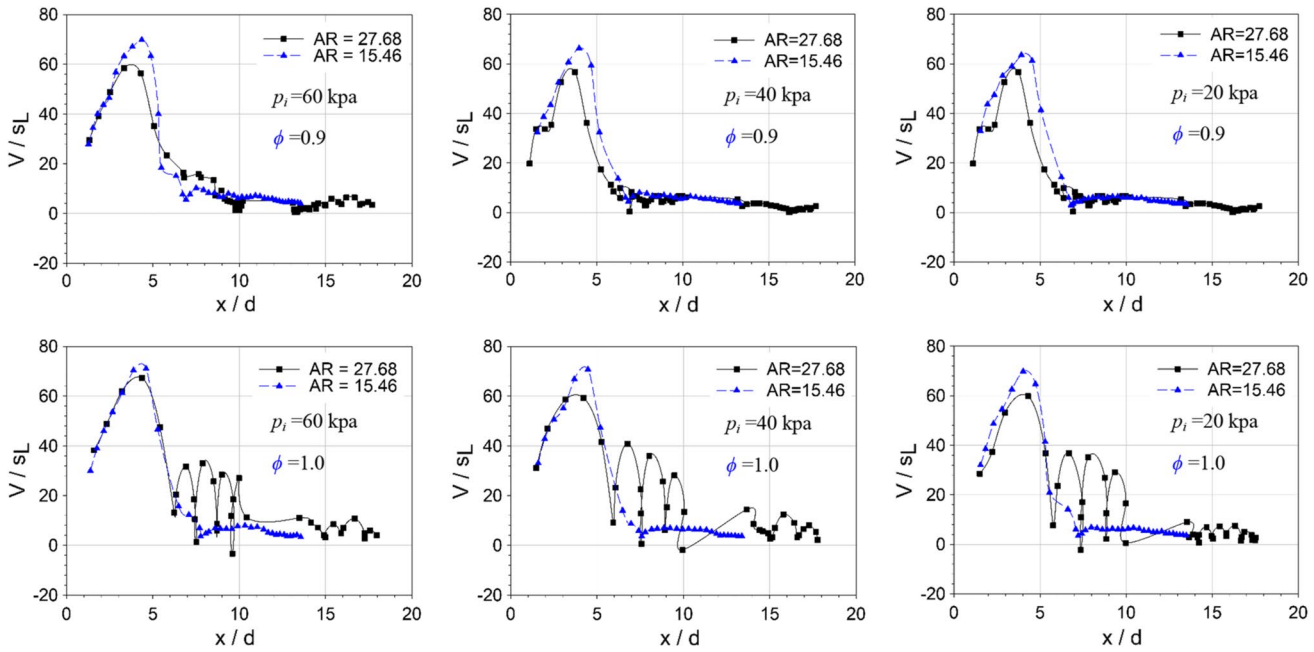

Fig. 4 Comparison of experimental results of the flame velocity along the tube axis obtained inside tubes with aspect ratios of 27.68 [This work] and 15.46 [39]

context, the work of Yu et al. [30], Yang et al. [35] and by Zheng et al. [26] should be mentioned. In these work, H_2–CO [30, 35] and H_2–CH_4 [26] fuel mixtures were considered. It can be observed that the high amplitude velocity oscillations occur in mixtures with higher laminar flame velocities, which is related to H_2 volume concentrations of at least 50%. However, as will be seen later, the aspect ratio also plays a role.

Since the laminar flame velocity is higher for mixtures with $\phi = 1.0$ and $\phi = 1.1$, it can be concluded from the results of the present work that the flame velocity variations with high amplitude are related to the laminar flame velocity of the fuel–air mixture. The relative increase of laminar flame velocity (Δs_L), using the value of s_L for $\phi = 0.8$ as a reference, is shown in Table 1. It is noticeable that for an initial pressure of 60 kPa, the value of Δs_L is 27.0% for $\phi = 1.1$ and 25.3% for $\phi = 1.0$. The value of Δs_L decreases for lower pressures. Nevertheless, it is always above 19% for $\phi = 1.0$ and higher for $\phi = 1.1$.

4.2 Boundary conditions

In the present work, flame velocity oscillations with high amplitude were determined for a closed tube for ethanol–air mixtures. When analyzing the results of Yu et al. [30] for H_2–CO–air mixtures propagating inside a closed duct with AR = 10, Xiao et al. [21, 53] for hydrogen–air mixtures with AR = 6.47 and Shen et al. [51] also for hydrogen–air mixtures with AR = 12, high amplitude velocity oscillations were also found.

However, for similar H_2–CO–air mixtures in half-open ducts the data of Yu et al. [28, 29] and Yang et al. [36] for AR = 10 and AR = 20, respectively, show no high amplitude flame velocity oscillations. However, there is a relatively slow variation of the flame tip velocity in the work of Yang et al. [36]. Another study by Yang et al. [35] can also be considered. They observed the behavior of flame propagation of H_2–CO–air mixtures in a closed duct and in a half-open duct with AR = 10. The high amplitude velocity oscillations are observed only for the closed duct. Thus, these oscillations occur for closed ducts and not for half-open ducts.

4.3 Internal pressure

Another variable related to the manifestation of the high amplitude velocity oscillations is the increase of the internal pressure along the duct with small variations. This statement can be better understood by comparing the pressure signals registered in the works of Yu et al. [29, 30] and Yang et al. [35]. In these work, it is found that for a closed duct the overall effect is that the internal pressure always increases in the cases where high amplitude velocity oscillations occur. For half-open ducts, on the other hand, the internal pressure reaches a maximum value and then begins to decrease and fluctuate. A schematic representation of this behavior can be found in Fig. 5. The pressure increase (Δp) shown in this figure is the difference between the initial pressure and the pressure evolution inside the duct as the flame propagates.

Another observation can be made by analyzing the results of Zheng et al. [26], who studied H_2–CH_4–air mixtures propagating in closed ducts. It is observed that for the mixture exhibiting high amplitude velocity oscillations the internal pressure always increases for small fluctuations. Therefore, the internal pressure and the high amplitude velocity oscillations are causally related.

Table 1 Characteristic time for flattened flame front formation (t_{flat}) of ethanol–air mixtures at different initial pressures and equivalence ratios inside a tube with high aspect ratio AR = 27.68 [This work] and Comparison with results obtained inside a tube with AR = 15.46 [39]

p (kPa)	ϕ[a]	τ_{wall}	s_L (cm/s)	Δs_L(%)	AR = 27.68		AR = 15.46	
					$t_{flat} = d_f/s_L$ (s)		$t_{flat} = d_f/s_L$ (s)	
60	0.80	0.250	38.22	+0.00	1.73	±0.12	–	–
60	0.90	0.238	44.36	+16.0	1.55	±0.03	1.19	±0.01
60	1.00	0.230	48.50	+25.3	1.53	±0.03	1.12	±0.04
60	1.10	0.227	48.53	+27.0	1.55	±0.04	1.09	±0.04
40	0.80	0.251	41.79	+0.00	1.24	±0.24	–	–
40	0.90	0.239	48.05	+15.0	1.20	±0.22	1.09	±0.01
40	1.00	0.231	51.72	+23.8	1.43	±0.01	1.04	±0.01
40	1.10	0.227	52.11	+24.7	1.45	±0.02	1.03	±0.02
20	0.80	0.233	47.59	+0.00	1.38	±0.10	–	–
20	0.90	0.240	53.79	+13.0	1.26	±0.00	0.96	±0.01
20	1.00	0.232	57.08	+19.0	1.29	±0.02	0.94	±0.00
20	1.10	0.229	57.44	+20.7	1.31	±0.02	0.91	±0.02

[a]Uncertainty is equal to 0.014 with respect to the equivalence ratio

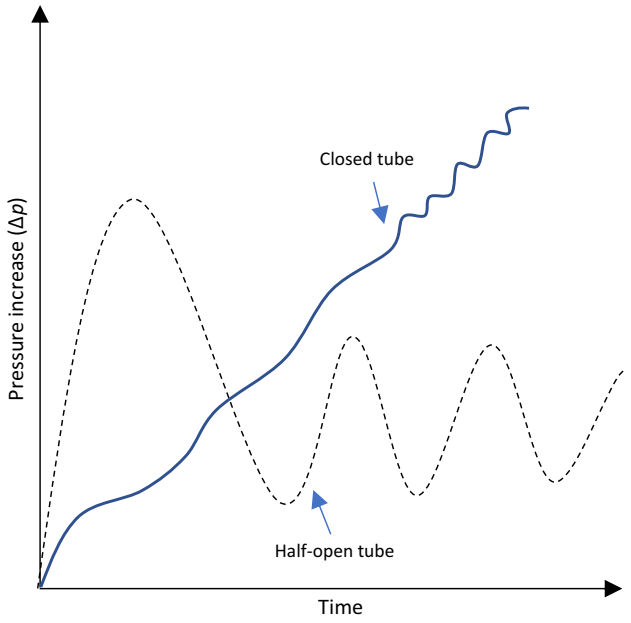

Fig. 5 Schematic representation of the internal pressure behavior for tubes closed and both ends and tubes closed only at the ignition end

4.4 Aspect ratio

The aspect ratio of the tube or duct is also an important parameter for the manifestation of high amplitude velocity oscillations. This statement is confirmed by comparing the current results with the authors' previous work [39]. In the authors' previous work, the ethanol–air deflagrations were studied in a closed tube with AR = 15.46. In that work, the initial pressures were 20, 40, and 60 kPa and the equivalence ratios ranged from 0.9 to 1.4. The results did not show the velocity oscillations observed in the present work (AR = 27.68) for $\phi = 1.0$ and $\phi = 1.1$. This observation can be confirmed by analyzing the results of Zheng et al. [26], who considered an aspect ratio of 5 to 20. In their work, it can be observed that the high amplitude velocity oscillation manifests itself for AR > 5. It is important to note that the value of laminar flame velocity is also important.

In summary, high amplitude velocity oscillations occur at equivalence ratios representing sufficiently high laminar flame velocities for closed tubes (or ducts), they are causally related to the evolution of pressure inside the tube (or duct), and they occur at sufficiently high aspect ratios.

4.5 The distance to flattened flame front

Another important experimental parameter is the axial distance traveled by the flame to the point where the flattened flame forms (d_f). This length can be converted into a characteristic time by dividing it by s_L. Thus, d_f and s_L define a characteristic time, as shown in Eq. (21).

$$t_{flat} = \frac{d_f}{s_L} \tag{21}$$

The distances d_f were measured using the videos obtained in the experimental tests, then the characteristic time t_{flat} was determined from Eq. (21). The results of this procedure are shown in Table 1 and are compared with those obtained in the authors' previous work [39]. It can be observed that there is a trend towards higher values of t_{flat} for the tube with higher aspect ratio. This means that the flame takes longer to flatten for tubes with higher aspect ratio.

As explained by Ponizy et al. [15], the cause of the flattening of the flame front is related to the backward motion of the combustion products. The backward motion starts near the ignition end, where the flame skirt first contacts the lateral tube walls. Then the backward motion "catches" the flame front as the mixture decreases in the radial direction while the flame also moves in the axial direction.

The high amplitudes of the velocity oscillations are related to the interaction with pressure waves, as shown by the numerical simulations of Xiao et al. [54]. Once the flame skirt touches the side walls of the tube, the simulations show that rarefaction waves are generated, and shock waves are produced in the later stages of flame propagation due to the interaction with pressure waves. In the same work, Xiao et al. [54] showed that Rayleigh–Taylor instability develops for sufficiently large aspect ratios.

To provide better context, the characteristic time and d_f were obtained from published experimental data. The collected data are listed in Table S.1 in the supplementary material. GetData Graph Digitizer software [55] was used to obtain numerical values for distance traveled from graphs published in the articles. Laminar combustion velocities were determined using Cantera software [42] in conjunction with the San Diego mechanism [56]. The t_{flat} and the d_f for different conditions are shown in Fig. 6. It can be observed that the t_{flat} decreases for mixtures with higher laminar flame velocities and the relationship between s_L and t_{flat} can be represented by a potential function. A correlation could be proposed for each aspect ratio. However, in some cases there is not enough experimental data to do this in a reliable way. The obtained correlations for closed ducts with AR = 6.46 and for half-open ducts with AR = 10.0 have the form shown in Eq. (22) and their information is given in Table 2.

$$t_{flat} = A s_L^B \tag{22}$$

It can be seen in Table 2 that the squared correlation coefficient (R^2) is always greater than 0.95 for the cases considered, which means that there is a very good correlation.

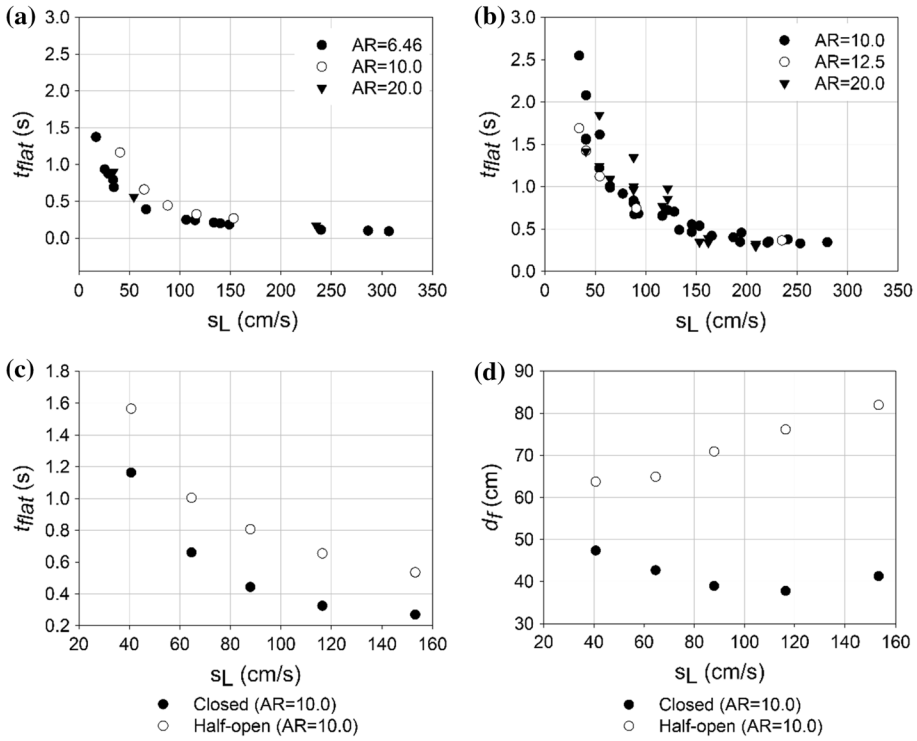

Fig. 6 Experimental values of t_{flat} and d_f obtained from published works. **a** Closed ducts with different AR [20, 22, 23, 26, 35, 60]; **b** Half-open ducts with different AR [27, 29, 35, 36]; **c** t_{flat} for closed vs half-open ducts for equal AR; **d** d_f for closed vs half-open ducts for equal AR [35]

Table 2 Correlations for characteristic time for flattened flame front formation (t_{flat}) for experimental data obtained in closed ducts with AR = 6.46 [20, 22, 23, 60] and in half-open ducts with AR = 10.0 [27, 29, 35, 36]

AR	End	*A*	*B*	MRE (%)	R^2
6.46	Closed	20.0985	−0.9374	2.68	0.9986
10.0	Half-open	51.4955	−0.9202	9.99	0.9512

MRE, Mean relative error

Also, the mean relative errors (MRE) are less than 3% for the closed ducts and less than 10% for the half-open ducts. This analysis proves that $t_{flat} = d_f/s_L$, as defined in Eq. (21), can be used together with s_L to determine the distance at which the flame front is flattened, d_f.

Analyzing the experimental data obtained by Yang et al. [35] in a duct with AR = 10.0, first with the duct closed and then with the duct half-open, it can be seen in Fig. 6c that the t_{flat} is always higher with the duct half-open. This observation is also confirmed by comparing Fig. 6a with Fig. 6b. Another interesting observation comes from Fig. 6d, where the values of d_f have been plotted against s_L. It can be clearly seen that increasing s_L in the closed duct causes a decrease in d_f, while increasing s_L in the half-open duct causes an increase in d_f.

The relationship between t_{flat} and fundamental combustion theory can be obtained by adopting the laminar flame velocity expression shown in Eq. (23) given by Law [57].

$$s_L \sim p^{\left(\frac{n}{2}-1\right)}\left[\left(\lambda/c_p\right)_b e^{-\frac{E_a}{RT_b}}\right]^{1/2} \tag{23}$$

In the above equation, p is pressure, n is reaction order, λ is thermal conductivity, c_p is heat capacity at constant pressure, E_a is activation energy, R is universal gas constant, and T_b is adiabatic flame temperature. Therefore, the t_{flat} can also be related to the properties of the mixture, as shown in Eq. (24).

$$t_{flat} \sim \mathrm{Ap}^{B\left(\frac{n}{2}-1\right)}\left[\left(\lambda/c_p\right)_b^B e^{-B\frac{E_a}{RT_b}}\right]^{1/2} \tag{24}$$

Analyzing Eq. (24), it is observed that the influence of the initial pressure is negligible when the reaction order is $n \sim 2$. Since B is negative (see Table 2), this means that mixtures with higher activation energies produce higher t_{flat}. Moreover, the influence of mixture properties is reversed in the sense that $(\lambda/c_p)^B = (c_p/\lambda)^{-B}$. Therefore, a mixture with higher values of the ratio (c_p/λ) produces higher values of t_{flat}. Note that higher values of t_{flat} mean that the flame travels longer inside the tube before touching the sidewalls. The fundamental relationship between t_{flat} and the properties of the mixture will be further explored in a future work.

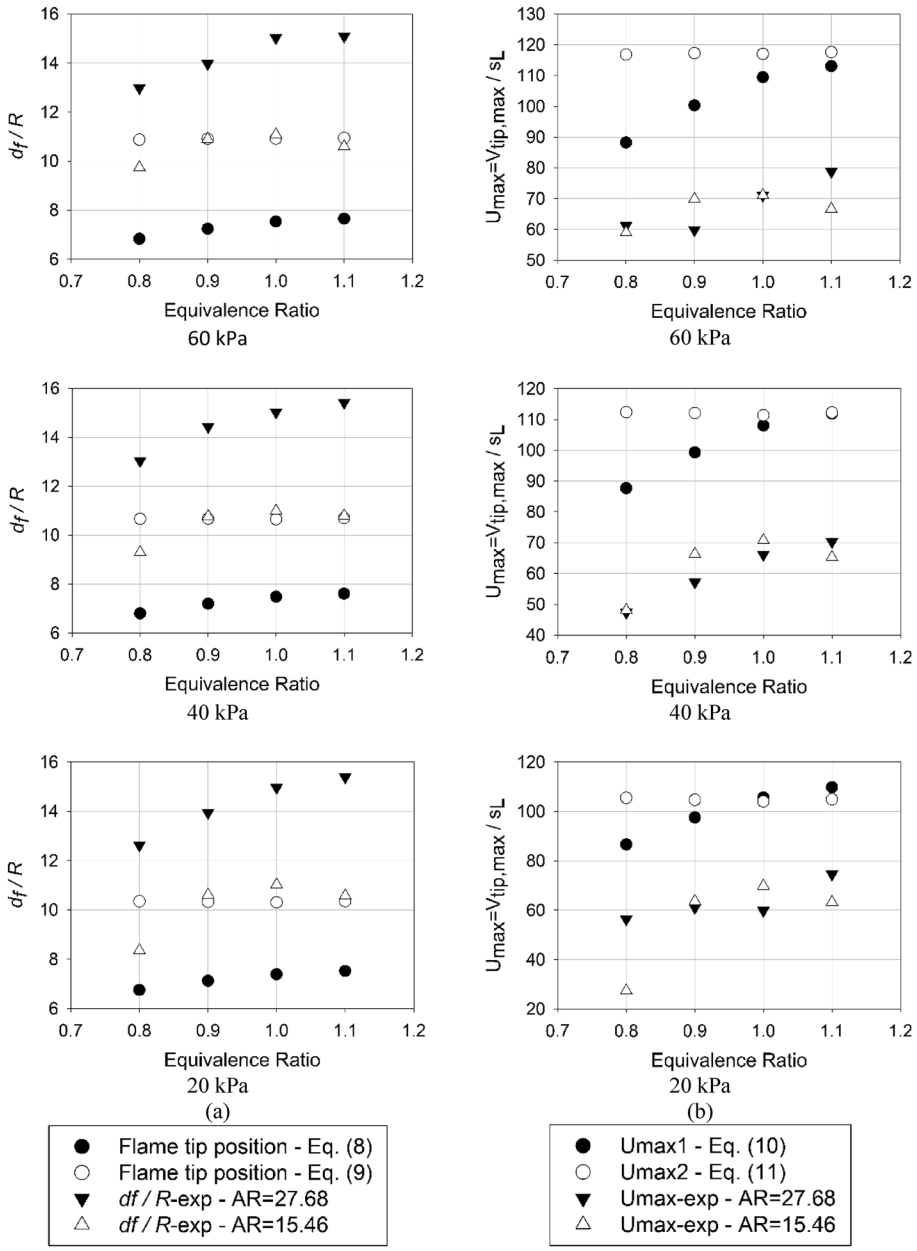

Fig. 7 Comparison with theoretical calculations for different initial pressures and ϕ for aspect ratios of 27.68 [This work] and 15.46 [39]. **a** Calculated flame tip position at τ_{wall} vs experimental d_f/R; **b** Calculated maximum flame tip velocity vs experimental maximum velocity

4.6 Comparison with theoretical calculations

Finally, the theory developed by Valiev et al. [8] is used to determine the maximum flame velocities and the distance traveled by the flame tip at the moment when the flame skirt touches the side walls of the tube. These calculations are compared with the experimental data obtained in the present work with AR = 27.68 and with the experimental data obtained in the authors' previous work with AR = 15.46 [39] for the distance at which the flame front flattens. The results of these comparisons are shown in Fig. 7.

It is important to note that the differential equations established by Valiev et al. contain a linear term and a nonlinear term. The linear term promotes acceleration of the flame, while the nonlinear term decelerates the flame. Then Valiev et al. neglected the nonlinear term and obtained the solutions given by Eqs. (8) and (10). On the other hand, if the nonlinear term is taken into account, the solutions given by Eqs. (9) and (11) are obtained. Since the differential equations were integrated for these two limiting cases, Fig. 7 shows two values for the position of the flame tip and the maximum velocity of the flame tip.

It can be seen in Fig. 7 that the flame tip position determined by Eq. (9) is close to the experimental values of d_f for the tube with AR = 15.46. On the other hand, the values of d_f determined in the present work are larger than those determined by theory. Moreover, the maximum flame speed determined by the theory is larger than the experimental

values for both aspect ratios. However, the order of magnitude is correct in both cases.

The results obtained by Quines et al. [58] show that the experimental U_{max} is lower than the calculated U_{max} for methane ($0.6 \leq \phi \leq 1.3$). In the case of acetylene with $\phi \leq 1$, the calculated and experimental U_{max} are well approximated. However, for acetylene with $\phi > 1$, it is observed that the calculated U_{max} is larger than the experimental one. For the same syngas with compositions $0.3H_2 + 0.7CO$ and $0.5H_2 + 0.5CO$, it was also observed that for $0.9 \leq \phi \leq 3.0$ the experimental U_{max} is larger than the calculated one. In a previous work, Silveira and Mendiburu [59] compared the experimental ratios d_f/d_h with the ratios resulting from the application of the theory of Valiev et al. The minimum relative error was 0.58% obtained for acetylene, the maximum relative error was 64.88% obtained for hydrogen, and the average value of the relative errors was 28.21%.

Future work will determine the value of d_f for fuel mixtures that can produce a wide range of values of s_L, and for different aspect ratios. This type of data will allow further investigation of the observations made in the present work.

5 Conclusions

Experiments were performed to observe the behavior of flame propagation of ethanol–air mixtures in a tube closed at both ends with a high aspect ratio of 27.68. The experiments were performed for equivalence ratios between 0.8 and 1.1 and for initial pressures between 20 and 60 kPa.

It was observed that the velocity oscillated in a wider interval for the stoichiometric and slightly rich mixtures. These oscillations did not occur in a previous study with aspect ratio of 15.46 with the same mixtures. These velocity oscillations occur when the mixture has a sufficiently high laminar flame velocity, when the tube is closed, and when the aspect ratio is sufficiently high. Moreover, the velocity oscillations are closely related to the pressure oscillations inside the tube, suggesting that they are the product of an interaction with pressure waves.

The distance traveled by the flame tip to the moment when the flattened flame front forms was measured experimentally, and a characteristic time was defined based on this distance ($t_{flat} = d_f/s_L$). Comparison of the experimental results of the present work (aspect ratio 27.68) with the results of a previous work (aspect ratio 15.46) shows that the t_{flat} is lower for the higher aspect ratio. The characteristic time was also taken from published experimental work and it was confirmed that it has lower values for higher aspect ratios and for half-open ducts.

Finally, the theoretical calculations for the position of the flame tip show results that approximate well the experimental values from the previous work. However, they underestimate the experimental results of the present work. For the calculated maximum velocities, the experimental results were always lower.

Supplementary Information The online version contains supplementary material available at https://doi.org/10.1007/s40430-022-04006-8.

Acknowledgements The authors are grateful to CNPq (Conselho Nacional de Desenvolvimento Científico e Tecnológico) for supporting this work through Project 423369/2018-0 and to FAPERGS (*Fundação de Amparo à Pesquisa do Estado de Rio Grande do Sul*) for supporting this work through Project 21/2551-0000677-3. The authors are grateful to FAPESP (*Fundação de Amparo à Pesquisa do Estado de São Paulo*) for support of this work through Projects 2015/23351-9 and 2015/25435-5.

References

1. Cavalett O, Chagas MF, Seabra JEA, Bonomi A (2013) Comparative LCA of ethanol versus gasoline in Brazil using different LCIA methods. Int J Life Cycle Assess 18:647–658. https://doi.org/10.1007/s11367-012-0465-0
2. Seabra JEA, Macedo IC, Chum HL, Faroni CE, Sarto CA (2011) Life cycle assessment of Brazilian sugarcane products: GHG emissions and energy use. Biofuels Bioprod Biorefining 5:519–532. https://doi.org/10.1002/bbb.289
3. Wang L, Quiceno R, Price C, Malpas R, Woods J (2014) Economic and GHG emissions analyses for sugarcane ethanol in Brazil: looking forward. Renew Sustain Energy Rev 40:571–582. https://doi.org/10.1016/j.rser.2014.07.212
4. Pereira LG, Cavalett O, Bonomi A, Zhang Y, Warner E, Chum HL (2019) Comparison of biofuel life-cycle GHG emissions assessment tools: the case studies of ethanol produced from sugarcane, corn, and wheat. Renew Sustain Energy Rev 110:1–12. https://doi.org/10.1016/j.rser.2019.04.043
5. Coronado CJR, Carvalho JA, Andrade JC, Mendiburu AZ, Cortez EV, Carvalho FS et al (2014) Flammability limits of hydrated and anhydrous ethanol at reduced pressures in aeronautical applications. J Hazard Mater 280:174–184. https://doi.org/10.1016/j.jhazmat.2014.07.063
6. Coronado C, Carvalho JA, Andrade JC, Cortez EV, Carvalho FS, Santos JC et al (2012) Flammability limits: a review with emphasis on ethanol for aeronautical applications and description of the experimental procedure. J Hazard Mater 241–242:32–54. https://doi.org/10.1016/j.jhazmat.2012.09.035
7. Mendiburu Zevallos AA, Ciccarelli G, Carvalho JA Jr (2018) DDT limits of ethanol–air in an obstacles-filled tube. Combust Sci Technol 00:1–16. https://doi.org/10.1080/00102202.2018.1477770
8. Valiev DM, Akkerman V, Kuznetsov M, Eriksson LE, Law CK, Bychkov V (2013) Influence of gas compression on flame acceleration in the early stage of burning in tubes. Combust Flame 160:97–111. https://doi.org/10.1016/j.combustflame.2012.09.002
9. De AG, De AC, Costa FDS (2015) Flameless compact combustion system for burning hydrous ethanol. Energy 89:158–167. https://doi.org/10.1016/j.energy.2015.07.049
10. Gárzon Lama LFM, Pizzuti L, Sotton J, Martins CA (2021) Experimental investigation of hydrous ethanol/air flame front instabilities at elevated temperature and pressures. Fuel. https://doi.org/10.1016/j.fuel.2020.119555
11. Clanet C, Searby G (1996) On the tulip flame phenomenon. Combust Flame 105:225

12. Gonzalez M, Borghi R, Saouab A (1992) Interaction of a flame front with its self-generated flow in an enclosure: the "tulip flame" phenomenon. Combust Flame 88:201–220. https://doi.org/10.1016/0010-2180(92)90052-Q
13. Konnov AA, Dyakov IV (2005) Measurement of propagation speeds in adiabatic cellular premixed flames of $CH_4 + O_2 + CO_2$. Exp Therm Fluid Sci 29:901–907. https://doi.org/10.1016/j.expthermflusci.2005.01.005
14. Jiang L, Gu C, Zhou G, Li F, Wang Q (2020) Cellular instabilities of n-butane/air flat flames probing by PLIF-OH and PLIF-CH_2O laser diagnosis. Exp Therm Fluid Sci. https://doi.org/10.1016/j.expthermflusci.2020.110155
15. Ponizy B, Claverie A, Veyssière B (2014) Tulip flame—the mechanism of flame front inversion. Combust Flame 161:3051–3062. https://doi.org/10.1016/j.combustflame.2014.06.001
16. Akkerman V, Bychkov V, Petchenko A, Eriksson LE (2006) Accelerating flames in cylindrical tubes with nonslip at the walls. Combust Flame 145:206–219. https://doi.org/10.1016/j.combustflame.2005.10.011
17. Bychkov V, Akkerman V, Fru G, Petchenko A, Eriksson L-E (2007) Flame acceleration in the early stages of burning in tubes. Combust Flame 150:263–276. https://doi.org/10.1016/j.combustflame.2007.01.004
18. Bychkov V, Petchenko A, Akkerman V, Eriksson LE (2005) Theory and modeling of accelerating flames in tubes. Phys Rev E Stat Nonlinear Soft Matter Phys 72:1–10. https://doi.org/10.1103/PhysRevE.72.046307
19. Xiao H, Wang Q, He X, Sun J, Shen X (2011) Experimental study on the behaviors and shape changes of premixed hydrogen–air flames propagating in horizontal duct. Int J Hydrog Energy 36:6325–6336. https://doi.org/10.1016/j.ijhydene.2011.02.049
20. Xiao H, Makarov D, Sun J, Molkov V (2012) Experimental and numerical investigation of premixed flame propagation with distorted tulip shape in a closed duct. Combust Flame 159:1523–1538. https://doi.org/10.1016/j.combustflame.2011.12.003
21. Xiao H, Wang Q, Shen X, Guo S, Sun J (2013) An experimental study of distorted tulip flame formation in a closed duct. Combust Flame 160:1725–1728. https://doi.org/10.1016/j.combustflame.2013.03.011
22. Xiao H, An W, Duan Q, Sun J (2013) Dynamics of premixed hydrogen/air flame in a closed combustion vessel. Int J Hydrog Energy 38:12856–12864. https://doi.org/10.1016/j.ijhydene.2013.07.082
23. Xiao H, Duan Q, Jiang L, Sun J (2014) Effects of ignition location on premixed hydrogen/air flame propagation in a closed combustion tube. Int J Hydrog Energy 39:8557–8563. https://doi.org/10.1016/j.ijhydene.2014.03.164
24. Xiao H, Sun J, Chen P (2014) Experimental and numerical study of premixed hydrogen/air flame propagating in a combustion chamber. J Hazard Mater 268:132–139. https://doi.org/10.1016/j.jhazmat.2013.12.060
25. Shen X, Xu J, Wen JX (2021) Phenomenological characteristics of hydrogen/air premixed flame propagation in closed rectangular channels. Renew Energy 174:606–615. https://doi.org/10.1016/j.renene.2021.04.056
26. Zheng K, Yu M, Zheng L, Wen X, Chu T, Wang L (2017) Experimental study on premixed flame propagation of hydrogen/methane/air deflagration in closed ducts. Int J Hydrog Energy 42:5426–5438. https://doi.org/10.1016/j.ijhydene.2016.10.106
27. Yu M, Zheng K, Zheng L, Chu T (2015) Scale effects on premixed flame propagation of hydrogen/methane deflagration. Int J Hydrog Energy 40:13121–13133. https://doi.org/10.1016/j.ijhydene.2015.07.143
28. Yu M, Zheng K, Zheng L, Chu T, Guo P (2015) Effects of hydrogen addition on propagation characteristics of premixed methane/air flames. J Loss Prev Process Ind 34:1–9. https://doi.org/10.1016/j.jlp.2015.01.017
29. Yu M, Yang X, Zheng K, Zheng L, Wan S (2018) Experimental study of premixed syngas/air flame propagation in a half-open duct. Fuel 225:192–202. https://doi.org/10.1016/j.fuel.2018.03.127
30. Yu M, Yang X, Zheng K, Zheng L, Wen X (2018) Experimental study of premixed syngas/air flame deflagration in a closed duct. Int J Hydrog Energy 43:13676–13686. https://doi.org/10.1016/j.ijhydene.2018.05.103
31. Hariharan A, Wichman IS (2014) Premixed flame propagation and morphology in a constant volume combustion chamber. Combust Sci Technol 186:1025–1040. https://doi.org/10.1080/00102202.2014.897340
32. Hariharan A, Wichman IS (2015) Structure and propagation of premixed flames in a closed combustion chamber with multiple ignition sources. Combust Sci Technol 187:1562–1583. https://doi.org/10.1080/00102202.2015.1050554
33. Li J, Zhang P, Yuan L, Pan Z, Zhu Y (2017) Flame propagation and detonation initiation distance of ethylene/oxygen in narrow gap. Appl Therm Eng 110:1247–1282. https://doi.org/10.1016/j.applthermaleng.2016.09.037
34. Dunn-Rankin D, Sawyer RF (1998) Tulip flames: changes in shape of premixed flames propagating in closed tubes. Exp Fluids 24:130–140
35. Yang X, Yu M, Zheng K, Wan S, Wang L (2019) A comparative investigation of premixed flame propagation behavior of syngas–air mixtures in closed and half-open ducts. Energy 178:436–446. https://doi.org/10.1016/j.energy.2019.04.135
36. Yang X, Yu M, Zheng K, Wan S, Wang L (2019) An experimental investigation into the behavior of premixed flames of hydrogen/carbon monoxide/air mixtures in a half-open duct. Fuel 237:619–629. https://doi.org/10.1016/j.fuel.2018.10.055
37. Emami SD, Sulaiman SZ, Kasmani RM, Hamid MD, Che Hassan CR (2016) Effect of pipe configurations on flame propagation of hydrocarbons–air and hydrogen–air mixtures in a constant volume. J Loss Prev Process Ind 39:141–151. https://doi.org/10.1016/j.jlp.2015.11.005
38. Song Y, Zhang Y, Chen Y, Liu X, Fu M, Li Y (2021) Numerical investigation of effects on premixed hydrogen/air flame propagation in pipes with different contraction or expansion angles. J Loss Prev Process Ind 70:104201. https://doi.org/10.1016/j.jlp.2020.104201
39. Mendiburu Z, Serra AM, De CA, Engineering M, Ufrgs S, Leite RS et al (2019) Characterization of the flame front inversion of ethanol–air deflagrations inside a closed tube. Energy 187:1–12. https://doi.org/10.1016/j.energy.2019.115932
40. ASTM E-681 (2010) Standard test method for concentration limits of flammability of chemicals (vapors and gases). Am Soc Test Mater 09:1–12. https://doi.org/10.1520/E0681-09R15.2
41. Brown D (2002) Tracker—video analysis and modelling tool
42. Goodwin DG, Moffat HK, Speth RL (2018) Cantera: an object-oriented software toolkit for chemical kinetics, thermodynamics, and transport processes. https://doi.org/10.5281/zenodo.170284
43. Marinov N (1999) A detailed chemical kinetic model for high temperature ethanol oxidation. Int J Chem Kinet 31:183–220. https://doi.org/10.1002/(SICI)1097-4601(1999)31:3%3c183::AID-KIN3%3e3.0.CO;2-X
44. Mendiburu AZ, Lauermann CH, Hayashi TC, Mariños DJ, Rodrigues da Costa RB, Coronado CJR et al (2022) Ethanol as a renewable biofuel: combustion characteristics and application in engines. Energy 257:124688. https://doi.org/10.1016/j.energy.2022.124688
45. Ciccarelli G, Chaumeix N, Mendiburu AZ, Guessan KN, Comandini A (2019) Fast-flame limit for hydrogen/methane–air mixtures.

Proc Combust Inst 37:3661–3668. https://doi.org/10.1016/j.proci.2018.06.045
46. Barbosa JA, Coronado CJR, Tuna CE, Silva MH, Mendiburu AZ, Carvalho Junior JA et al (2021) Experimental determination of lower flammability limits of synthesized iso-paraffins (SIP), jet fuel and mixtures at atmospheric and reduced pressures with air. Fire Saf J. https://doi.org/10.1016/j.firesaf.2021.103276
47. Barbosa JA, Coronado CJR, de Andrade JC, Tuna CE, Silva MH, Carvalho Junior JA et al (2022) Experimental determination of upper flammability limits of synthesized iso-paraffins (SIP), Jet fuel and their mixtures with air at atmospheric and sub-atmospheric pressures. Process Saf Environ Prot 160:102–115. https://doi.org/10.1016/j.psep.2022.02.016
48. Carvalho JA, Mendiburu AZ, Coronado CJ, McQuay MQ (2018) Combustão aplicada. Editora da Universidade Federal de Santa Catarina, Florianópolis
49. Holman JP (2011) Experimental methods for engineers, 8th edn. Mc Graw Hill, New York
50. Gonzalez M (1996) Acoustic instability of a premixed flame propagating in a tube. Combust Flame 107:245–259. https://doi.org/10.1016/S0010-2180(96)00069-7
51. Shen X, Zhang C, Xiu G, Zhu H (2019) Evolution of premixed stoichiometric hydrogen/air flame in a closed duct. Energy 176:265–271. https://doi.org/10.1016/j.energy.2019.03.193
52. Shen X, He X, Sun J (2015) A comparative study on premixed hydrogen–air and propane–air flame propagations with tulip distortion in a closed duct. Fuel 161:248–253. https://doi.org/10.1016/j.fuel.2015.08.043
53. Xiao H, Duan Q, Sun J (2017) Premixed flame propagation in hydrogen explosions. Renew Sustain Energy Rev. https://doi.org/10.1016/j.rser.2017.06.008
54. Xiao H, Houim RW, Oran ES (2017) Effects of pressure waves on the stability of flames propagating in tubes. Proc Combust Inst 36:1577–1583. https://doi.org/10.1016/j.proci.2016.06.126
55. GetData. GetData Graph Digitizer 2018. http://getdata-graph-digitizer.com/index.php. Accessed 7 May 2018
56. University of California at San Diego. San Diego Mechanism 2019. https://web.eng.ucsd.edu/mae/groups/combustion/mechanism.html
57. Law CK (2006) Combustion physics. Cambridge University Press, New York
58. Quines R, Nzinga M, Mendiburu AZ (2021) Study of flame acceleration in closed and half-open ducts. In: Proceedings of 26th international congress mechanical engineering. ABCM. https://doi.org/10.26678/ABCM.COBEM2021.COB2021-0283
59. Silveira J, Mendiburu AZ (2020) Relevant parameters on the formation of tulip flames. In: Procceedings 18th Brazilian Congress Thermal Science Engineering. ABCM. https://doi.org/10.26678/ABCM.ENCIT2020.CIT20-0190
60. Jin K, Duan Q, Liew KM, Peng Z, Gong L, Sun J (2017) Experimental study on a comparison of typical premixed combustible gas–air flame propagation in a horizontal rectangular closed duct. J Hazard Mater 327:116–126. https://doi.org/10.1016/j.jhazmat.2016.12.050